

Morphology matters in immune cell chemotaxis: membrane asymmetry affects amplification

Matthew David Onsum^{1,5}, Kit Wong², Paul Herzmark², Henry R Bourne²
and Adam Paul Arkin^{3,4}

¹ Department of Mechanical Engineering, University of California, Berkeley, CA 94720, USA

² Department of Cellular and Molecular Pharmacology and Department of Medicine and The Cardiovascular Research Institute, University of California, San Francisco, CA 94143 USA

³ Howard Hughes Medical Institute, Department of Bioengineering, University of California, Berkeley, CA 94720, USA

⁴ Physical Biosciences Division, E O Lawrence Berkeley National Laboratory, Berkeley, CA 94720, USA

E-mail: aparkin@lbl.gov

Received 5 April 2006

Accepted for publication 1 September 2006

Published 25 September 2006

Online at stacks.iop.org/PhysBio/3/190

Abstract

A key mediator of eukaryotic chemotaxis is the asymmetric accumulation of phosphatidylinositol-3,4,5-triphosphate (PIP3) on the cell membrane. Recent work has focused on understanding how a shallow external gradient of chemoattractant leads to an amplified internal gradient of PIP3. In this paper we dissect what fraction of this amplification is derived biochemically by the signal transduction network and how much arises entirely from the effects of cell morphology. Here we identify and formalize the role of morphology in signal detection and demonstrate its effects through simulation and experiments. Our key result is that an asymmetric distribution of membrane accounts for approximately one-half of the measured amplification from ligand concentration to PIP3 production. We also show that the underlying biochemical network behaves as a linear amplifier in the micropipette assay.

 This article features online multimedia enhancements

Introduction

Chemotaxis is the directed migration of a cell in response to a gradient of chemical stimulus from the external environment. It involves the sensing and processing of signals by many contributing effectors leading to the generation of motion toward a source. Eukaryotic chemotaxis is essential for leukocyte migration to sites of infection and tissue damage, guidance of axonal outgrowth to target cells in the development of the nervous system and the aggregation of the social amoeba *Dictyostelium discoideum* to form a multicellular structure. Remarkably, neutrophils and *Dictyostelium* can initiate chemotaxis in response to concentration differences

as low as 2% across their cell length [1] and use a relatively evolutionarily conserved pathway to do so.

Chemotaxis depends on the localized restructuring of the cytoskeleton to initiate motion. Most research points to phosphatidylinositol-3,4,5-triphosphate (PIP3) as the key mediator of this localized response of the cytoskeleton. PIP3 is a membrane-associated lipid product of the phosphatidylinositol-3-OH kinases (PI3Ks), which are activated by G-proteins during chemotaxis. PIP3 is one of the most upstream components of the known chemotaxis network to strongly localize toward the gradient; the internal gradient of PIP3 has been reported to be seven times greater than the external gradient of attractant [2] while receptors and G-protein subunits remain nearly uniformly distributed along the plasma membrane [3]. Additionally, PIP3 promotes the activity of Rac and Cdc42 (members of the Rho GTPase

⁵ Present address: Pathways Capability, AstraZeneca R&D Boston, Waltham, MA 02451, USA.

family) [4], which in turn, initiate actin polymerization at the leading edge by activating p21-activated kinases (PAK). Therefore the regulation of PIP3 is considered to play a central role in transducing shallow chemoattractant gradients into an amplified response that will initiate actin polymerization at the leading edge. Because of its central role in the chemotaxis pathway, recent research has focused on the regulators of PIP3 synthesis and degradation [5, 6].

To better understand how PIP3 acts in the ‘chemotaxis compass’, by directing pseudopod formation, there are systems-level features of the network that need to be quantified. In this paper, we are concerned with PIP3 amplification, which is the ratio of the per cent change in PIP3 production across the cell length to the per cent change in chemoattractant [7]. PIP3 amplification in gradient sensing could be achieved by a number of mechanisms, including cooperativity [8], zero-order ultrasensitivity and positive feedback [9–11]. An accurate measure of amplification will constrain the underlying gradient sensing mechanism.

Amplification of the external gradient of chemoattractant by the GPCR-driven PIP3 network has previously been reported in both neutrophil-like HL60s and *Dictyostelium* [2, 12]. In these studies amplification was measured first in naturally polarized cells and then again in cells that were treated with latrunculin, an actin polymerization inhibitor, to prevent polarization. In the latter case, the cells had a circular morphology. In both cell types the polarized cells had a higher value of amplification (as measured by the ratio of the internal gradient of PIP3 to the external attractant) than the circular cells. In the case of HL60s, the latrunculin-treated cells showed no amplification, while in *D. discoideum*, there was still PIP3 amplification, but it was much less than the untreated, polarized cell. It has been postulated that a polarized cell achieves higher amplification than a circular cell because actin is part of a biochemical feedback loop with PIP3, but there is no conclusive proof of this hypothesis [12]. However, the morphology of the polarized cell and the circular cell is quite different. Another hypothesis, then, is that the shape difference between the two morphologies is responsible for the amplification difference under the two conditions.

Since receptors are evenly distributed in the membrane [3], morphology will determine how receptors are distributed in the field of chemoattractant and this will affect amplification. Consider the morphologies in figure 1. Cells 1 and 2 are both circular, but cell 2 has more of its membrane oriented toward the gradient (illustrated by the darker shading near the front). Such an asymmetric distribution of membrane could be the result of membrane ruffling at the leading edge or the greater height of the cell at its front than at its back. Since more receptors are in a higher concentration of attractant, it would not be clear if the measured PIP3 amplification is a result of the biochemical network or the localization of receptors. Cell 3, on the other hand, has a uniform distribution of membrane but it is polarized in the direction of the gradient. The elongated shape of cell 3 will put more receptors at the leading edge in a higher concentration of attractant than cell 1, and likewise the receptors at the back will be in a lower concentration. Therefore PIP3 will be more localized to the front in a polarized cell.

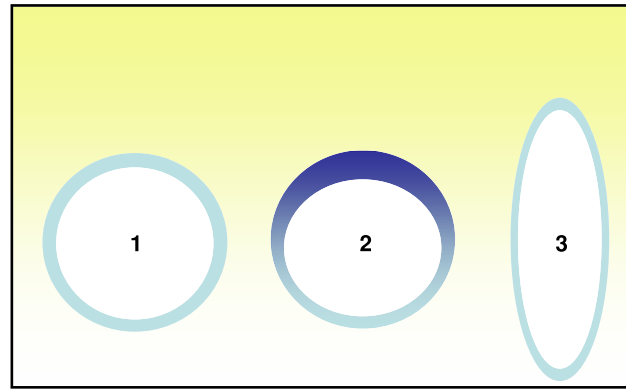


Figure 1. Morphology affects signal localization by placing receptors in a region of higher chemoattractant concentration. Cell 2 achieves higher signal localization than cell 1 by an asymmetric distribution of plasma membrane (represented by darker shading). Cell 3 localizes the signal by elongating in the direction of the gradient thereby enhancing the difference of measured chemoattractant from front to back.

In this paper, we formalize the role of morphology in signal amplification and demonstrate how its effects can be parsed out from the biochemical amplification. We are not considering the mechanisms that allow a cell to rapidly respond to changing gradients of attractant, rather, we focus on how morphology affects measures of amplification. First, we measure the localization of PIP3 and receptors in chemotaxing HL60s and parse out what fraction of the observed amplification is a result of the network and how much derives from the morphology. In contrast to prior work that measured PIP3 amplification [2, 12], we have specifically accounted for the distribution of receptors, membrane and cell shape and therefore have a more precise measure of amplification afforded by the signaling network. Second, we found that shape polarity does not affect amplification. A systems-level consequence of this finding is that the underlying biochemical network behaves as a linear amplifier in the micropipette assay.

Materials and methods

Reagents

Human fibronectin was obtained from BD BioSciences (Palo Alto, CA). Human albumin (low endotoxin) and fMLP were from Sigma (St Louis, MO). The electroporation chamber (Model Series 1600) was from GIBCO-BRL. Texas Red was from Molecular Probe.

DNA constructs

PCR fragments of CPF-CAAX from pEX-EF1-CFP-Kras4b-C19 (Alliance for Cellular Signaling) and PH-Akt-YFP in pEYFP [20, 21] containing appropriate flanking cloning sites were cloned into FuPw vector (Todd Branon) for lentivirus production. Plasmid for C5aR is described in [22].

Cell culture and transfection

Procedures for cultivation and differentiation of HL60 have been described in [12]. For transient transfections, differentiated HL60 cells (on day 6 after addition of DMSO) were washed once in RPMI-HEPES and resuspended in the same medium to a final concentration of 10^8 ml^{-1} . DNA was then added to the cells (30 μg of PH-Akt-YFP DNA, plus 50 μg of other constructs to be cotransfected); the cell-DNA mixture was incubated for 10 min at room temperature, transferred to electroporation cuvettes and subjected to an electroporation pulse on ice at 310 V, 1180 μF and low resistance. Transfected cells were allowed to recover for 10 min at room temperature and then transferred to 20 ml complete medium. Subsequent assays were performed 16–24 h after transfection.

For lentiviral infections, pVSV.G, pCMVD8, 9 and FuPw-CFP-CAAX or FuPw-PH-Akt-YFP were co-transfected into HEK cells using Lipofectamine 2000 (Invitrogen) according to manufacturer's protocol. Supernatants were harvested at 48 h after transfection, cleared and concentrated using Centriprep spin columns (Amicon). 28 ml of supernatant was typically concentrated into 1–2 ml.

To generate HL60 cells expressing CPF-CAAX or PH-Akt-YFP, concentrate containing lentiviral particles was added to undifferentiated HL60 cells. Seven days after infection, cells were FAC sorted for CFP/YFP expression and cultured and differentiated as described above.

Microscopic analysis

Microscopic analysis of cells stimulated with a uniform concentration or a point source of chemoattractant was performed as described in [3]. All images were acquired at room temperature with a Nikon inverted, Eclipse TE200 microscope with a 60 \times Plan Apo lens ($\text{NA} = 1.4$) and a cooled CCD camera (Roper Scientific). The microscope and camera were controlled with DeltaVision image acquisition software.

Assays

For 3D analysis in fixed cells, cells were subjected to stimulation with fMLP (100 nM) for 3 min. Cells were extracted by 0.5% Triton X-100 on ice for 1 min or 5 U ml^{-1} streptolysin-O for 10 min at room temperature, followed by 3.7% paraformaldehyde fixation.

Live cells were imaged after stimulation by a point source of chemoattractant from a micropipette (Femtotips) containing 10 μM fMLP, as described in [13].

Control experiments were performed to test for photobleaching. Cells in the chemotaxis assay were exposed to fMLP and followed by phase contrast and fluorescence microscopy for 10 min. Images of the CFP CAAX, PH-Akt-YFP and Texas Red distributions were captured in 10 s intervals for a total of 61 images in each channel. Each fluorescent marker required 1 s of fluorescence excitation, which gives 61 s of fluorescent excitation for each marker in this assay. Prior to exposure to fMLP, these same cells were exposed for an additional 61 s of fluorescence excitation

in each channel. Total cellular fluorescence was measured and found to remain nearly constant after the pre-exposure and after the chemotaxis assay. Thus, photobleaching did not seem to be a large effect in these experiments (data not shown).

Data analysis

All analyses were performed using MATLAB (Mathworks, Natick, MA). The cells were segmented using a combination of edge detection (from MATLAB's Image Processing Toolbox) and active contour methods [23]. While our segmentation algorithm is quite robust, it did miss some of the finer details of the cell boundary. However, these fine details, when included by hand, had a negligible effect on our results. After segmentation, the average intensity value of PH-AKT-YFP, CAAX-CFP and Texas Red/fmLP, in 5×5 pixel box at each boundary point was recorded. Statistical analyses (regression lines, *t*-tests, etc) were performed with the MATLAB Statistics Toolbox. In particular, we made use of the robust regression function *robustfit.m* (see [16] for more details) to calculate the slope of the input–output plots. Confidence intervals for the amplification values were calculated by first computing the standard error of the slope of the regression line (SE) and then multiplying by the upper critical value of the *t*-distribution for 95% confidence.

Results

Membrane localization affects amplification

Previously reported measures of PIP3 amplification implicitly assumed that the receptor distribution was constant [2]; however, it has been shown that membrane, and therefore receptors, accumulate at the leading edge of chemotaxing, neutrophil-like cells [3]. Clearly the localization of receptors at the front will lead to greater PIP3 localization and thus a higher value of amplification, though this apparent gain in amplification is not a direct result of the signal transduction network. In order to quantify this morphological effect, we first verified that there is indeed more membrane at the leading edge of stimulated cells. For this experiment we transfected HL60s with plasmids for chimera proteins of the C5a receptor fused with CFP (C5aR-CFP) to label the receptor distribution, and the pleckstrin homology domain of Akt linked with YFP (Ph-Akt-YFP) to measure PIP3 [13], which in this experiment labels the leading edge when the cell is exposed to chemoattractant. This combination of fluorescent markers had no detectable overlap in their emission bands. The cells were then uniformly exposed to 100 μM of the attractant f-Met-Leu-Phe (fMLP) for 3 min to induce PIP3 translocation and polarization, fixed and imaged in three dimensions with a deconvolution microscope. We then used custom image processing software to examine the colocalization of PH-Akt-YFP and C5aR-CFP. We extracted transverse sections through the cell at different heights above the coverslip and extracted the cell boundary. At each point on the boundary we recorded the intensity of Ph-Akt-YFP and C5aR-CFP. Figures 2(a) and (b) show the intensity images of the C5aR-CFP and PH-Akt-YFP channels from one Z-plane of one of

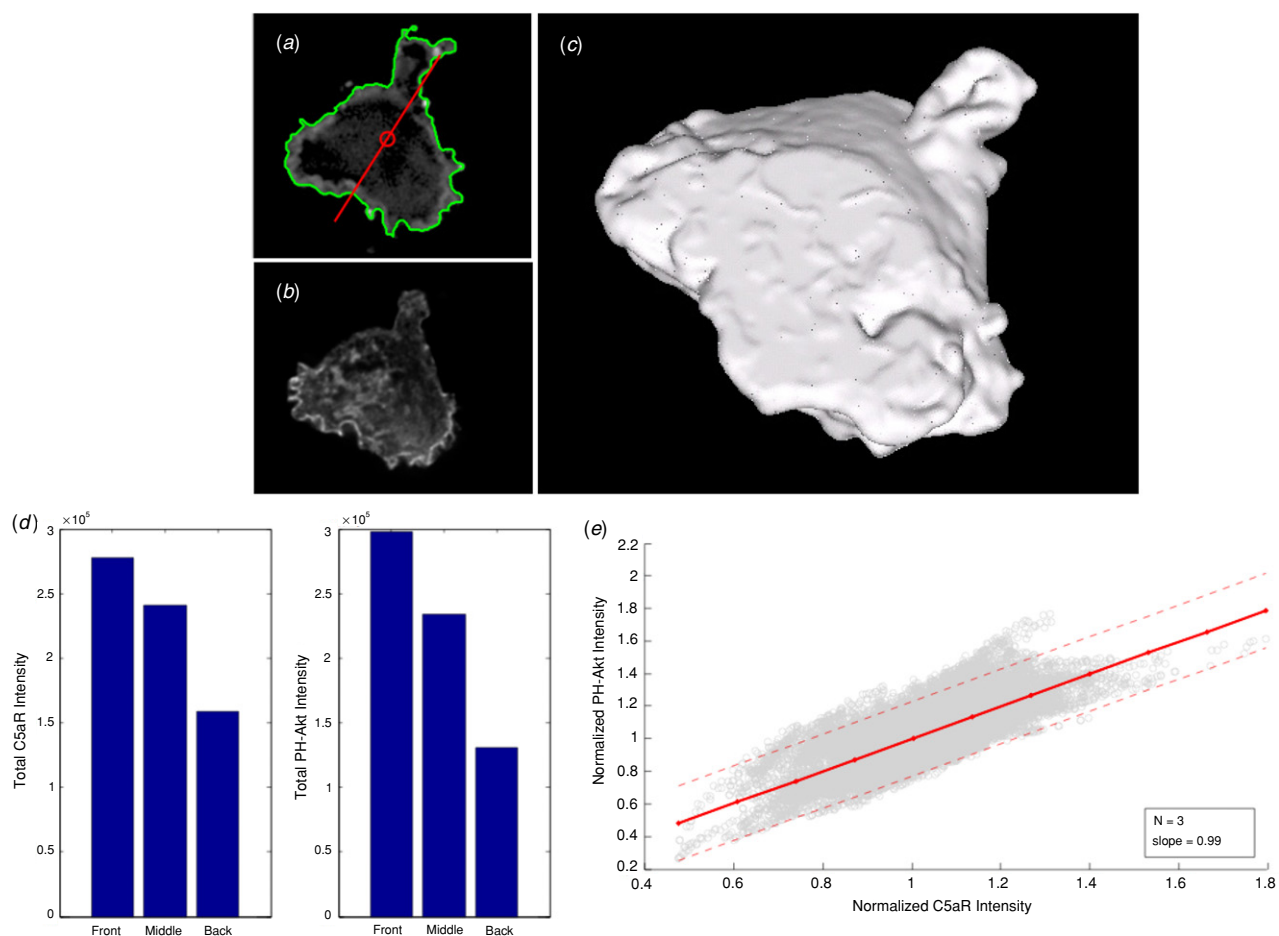


Figure 2. fMLP stimulated, chemokinesing HL60s have more receptors at the front than at the back. (a) An image of the C5aR-CFP distribution shown with segmented boundary (green), centroid (red circle) and axis of polarity (red dashed line). (b) An image of the PH-Akt-YFP distribution. (c) A three-dimensional reconstruction of cell morphology. (d) A comparison of the total C5aR and PH-Akt intensity at the front, middle and back of the cell. (e) The correlation of PH-Akt to C5aR-CFP for three cells. Solid line is the best-fit, linear approximation. Dashed lines are the 95% prediction intervals, that is, if another data point is collected then it will be between the two lines, with 95% confidence.

our experiments. Figure 2(a) also shows the computed cell boundary (green), centroid (red circle) and axis of polarity (red dashed line) for that image. Figure 2(c) shows a reconstruction of nearly the entire cell from its Z-stack. We could not extract the boundaries of the top five images of the cell because of excessive out-of-plane light, which is why the cell appears to have a flat top. We assessed the distribution of membrane/receptors and PH-Akt on the cell membrane from the front to the back of the cell by binning the recorded intensities at the cell membrane from all Z-stacks according to their distance from the cell front. We define the cell front as the point on the lamellipodium that has the maximum PH-Akt-YFP intensity. Figure 2(d) shows the total intensity in each of three bins from one of our experiments. The front bin contains all points on the cell membrane within one-third of the total cell length from cell front, the back bin contains all points greater than two-thirds of the cell length from the cell front and the middle bin contains the points in between. For the three cells considered, we found there to be on average $41 \pm 16\%$ more C5aR-CFP at the front than at the back.

Figure 2(e) shows a scatter plot of the intensities of C5aR-CFP versus PH-Akt-YFP for every image in the stack of three cells and the best-fit line. The slope of this line with 95% confidence is 0.99 ± 0.02 , which is insensitive to cell height. This result further demonstrates that there is strong correlation between the membrane and PIP3 distributions. Regions with a high membrane concentration had similarly high PIP3 concentration. While it was shown in [3] that there was more membrane at the front of a chemotaxing cell, we were the first to quantify this distribution.

Next we measured amplification in live cells chemotaxing up an fMLP gradient and assessed the effect of morphology on amplification. For these experiments we transfected HL60 cells with PH-Akt-YFP to label PIP3, the CAAX domain of KRAS fused to CFP (CFP-CAAX) to label the membrane distribution, and we used a micropipette with a mixture of fMLP and Texas Red to create a fluorescent gradient. This combination of fluorescent markers had no detectable overlap in their emission bands. We chose to use CFP-CAAX instead of C5aR-CFP for these experiments because we were able

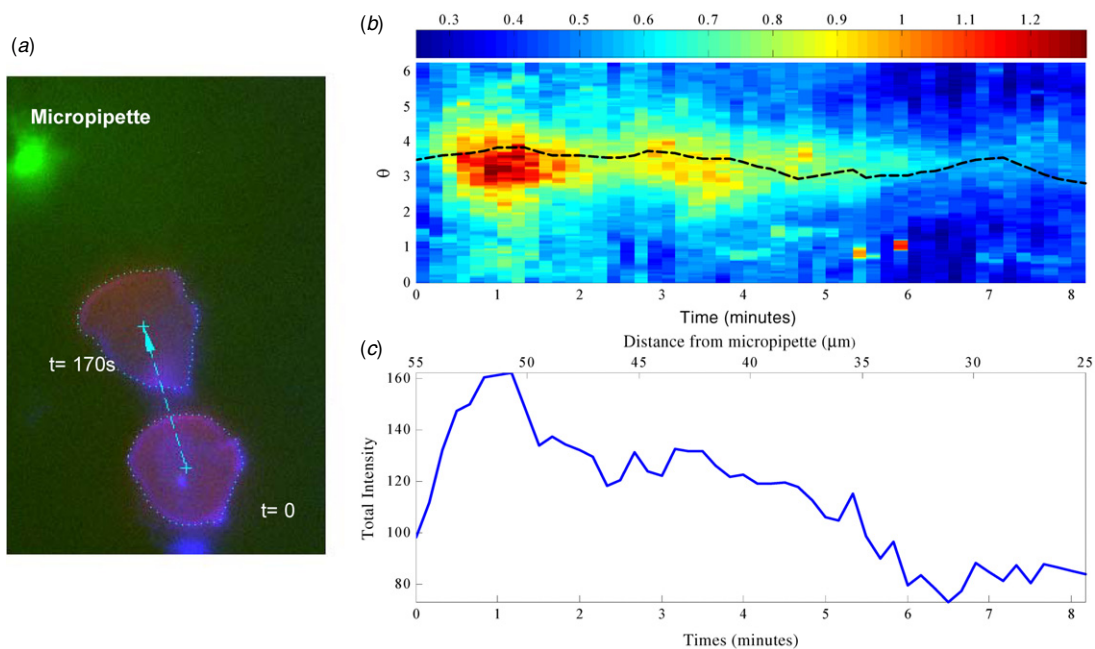


Figure 3. Analysis of PIP3 localization in a chemotaxing HL60. (a) A composite image taken from one experiment. PH-Akt-YFP distribution is in red, CFP-CAAX is in blue and the fMLP concentration is in green. (b) The signal dynamics for one micropipette experiment. The abscissa is time in minutes, the ordinate represents the location on the cell periphery and the color represents signal intensity. The black line is the point on the cell boundary receiving the highest fMLP concentration. (c) Total signal around the periphery of the cell.

to achieve higher transfection efficiency, which was vital for working with live cells.

For each frame of the experiment we segmented the cell boundary and recorded the intensity values of the CFP-CAAX, PH-Akt-YFP and fMLP/Texas Red at each point on the cell boundary. Figure 3(a) shows a composite image of one of our experiments: CFP-CAAX is displayed in blue, PH-Akt-YFP in red, the gradient is in green and the segmented cell boundary is shown with the dotted cyan line. Figure 3(b) shows the spatial and temporal dynamics of the PH-Akt-YFP intensity from one of our experiments. The x -axis is time (minutes), the y -axis represents points on perimeter of the cell, and the color corresponds to the normalized intensity of the PH-Akt-YFP at the boundary. The black dashed line represents the point on the cell's boundary that is exposed to the highest fMLP concentration; therefore, this line represents the path the cell should follow to the micropipette. Figure 3(c) shows the total signal intensity around the cell as a function of time (this is simply a column sum of the data in figure 3(b)) as well as distance to the micropipette (see scale on the top of figure 3(c)). We can plot signal intensity as a function of both time and distance since leukocytes travel at a constant velocity [14] (see supplementary figure 1 available at stacks.iop.org/PhysBio/3/190). We see that as the cell gets closer to the micropipette, the total PH-Akt-YFP intensity decreases, which may be due to desensitization of the receptors [15] (our control experiments demonstrated that this decrease in intensity was not due to photobleaching; see Materials and methods). For the analysis that follows we will only be interested in the maximum signal amplification (in this case

at time ~ 1 min); this will allow us to directly compare our results with the previous work [2, 12].

We now separate the biochemical amplification from the effects of an asymmetric distribution of membrane. Figure 4(a) shows the distribution of the PH-Akt-YFP intensity about the perimeter of the cell. The green line is the PH-Akt-YFP intensity, and the blue line is the PH-Akt-YFP signal normalized by the membrane signal. Figure 4(b) shows a scatter plot of the distribution of the two output signals against the fMLP distribution, with their respective best-fit lines. We see that the slope of the normalized PH-Akt-YFP signal (blue, slope = 1.8 ± 0.11) is less than the original PH-Akt-YFP signal (green, slope = 2.6 ± 0.14). This is a direct result of there being more membrane at the front of the cell.

Figure 4(c) shows the amplification calculation results for 11 of our 16 experiments (see appendix B for a discussion of the excluded experiments). Each experiment shows two values of amplification. The first value of amplification (white) is the per cent change in PH-Akt-YFP divided by the per cent change in fMLP across the cell. This is a similar calculation to what has been previously reported. The second value of amplification (gray) is the per cent change in PH-Akt-YFP normalized by CFP-CAAX divided by the per cent change in fMLP. We see that for each experiment the measured amplification decreased when we normalized the receptor distribution by a statistically significant amount (95% confidence intervals are shown). On average the normalized amplification is 3.25 ± 2.0 , and the unnormalized amplification is 5.34 ± 2.5 . These values are significantly different at the $P = 0.002$ level according to the paired T -test. This gives a 49% difference in the two measures of

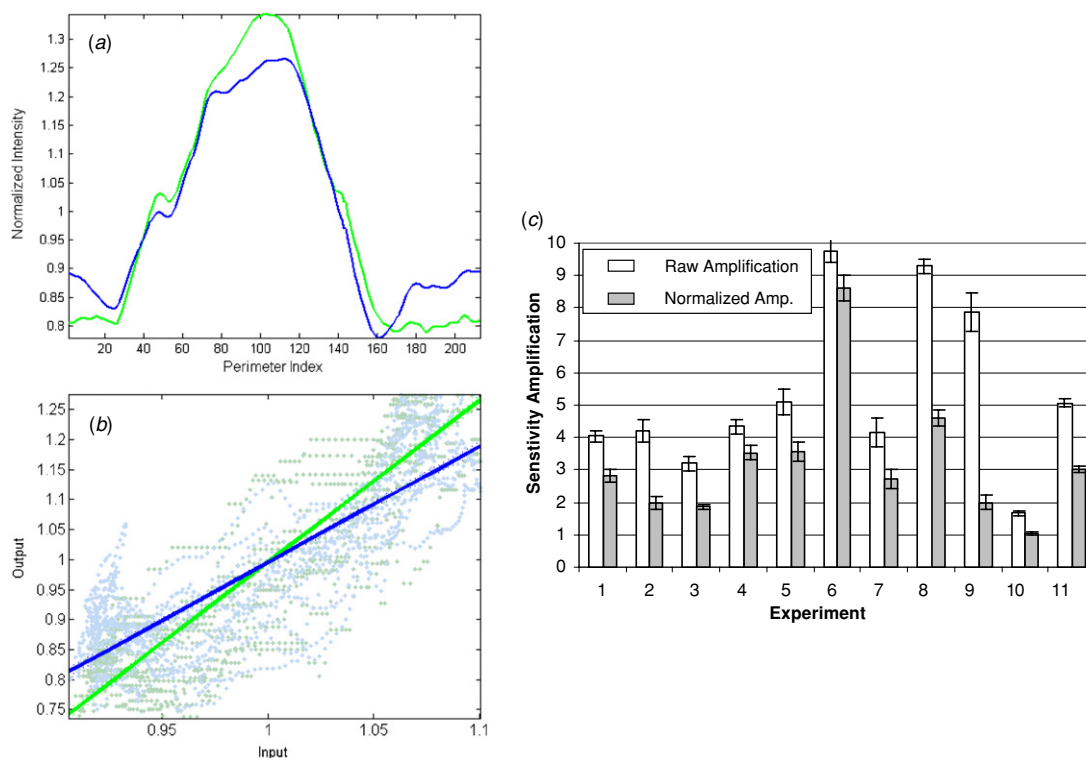


Figure 4. An asymmetric distribution of membrane gives the appearance of higher amplification. (a) The distribution of PH-Akt-YFP around the perimeter of one cell. The green line is the raw PH-Akt-YFP signal and the blue line was normalized by the membrane distribution. (b) Input–output plot of the data shown in (a). Blue and green dots are data points of the normalized and unnormalized PH-Akt-YFP values versus fMLP, respectively. Best-fit lines (solid) and 95% confidence intervals (dashed) are shown. (c) Amplification results for 11 cells, with 95% confidence intervals shown.

amplification. Our normalized amplification value agrees with the value reported for latrunculin-treated *D. discoideum* (3.1 ± 0.9) and our value of the unnormalized amplification falls within the range of values reported for polarized *D. discoideum* (7.1 ± 3.5) [2]. The implication of these results is that the amplification difference between polarized and unpolarized cells can be explained by the difference in membrane density. Additionally, the amplification results reported in [12] for polarized HL60s (approximately 6.3) are in agreement with our value for unnormalized amplification. Furthermore, their value of amplification in latrunculin-treated cells (approximately 1.3) also falls within our range of values for normalized amplification. While there is some agreement with our results and those presented in [12], our methods of data extraction are different. We used all of the data along the cell boundary to compute the change in PH-Akt from the front to the back of the cell. The authors of [12], on the other hand, used the peak intensity value at the front of the cell and the intensity value at the trailing edge to approximate the change in PH-Akt.

Amplification is not correlated with cell shape

In this section, we consider the effect of shape polarity. In appendix A, we derive conditions under which shape polarity will increase amplification. The key result is that if the biochemical network that transduces ligand to PIP3 acts

as a nonlinear amplifier then the polarity will increase the amplification of a linear gradient. Otherwise, if the network behaves linearly then there will be no appreciable gain in amplification.

To define the shape polarity of a chemotaxing HL60s we first segment the cell boundary, and then compute the best-fit ellipse to the boundary points. The ratio of the major and minor axes of the ellipse defines the shape polarity. Figures 5(a) and (b) show two cells with polarity of 1.2 and 1.9, respectively.

Figure 5(c) shows the association of polarity with the normalized amplification. The blue dashed line is a robust regression [16] through the data, and blue dotted lines are 95% confidence intervals on the prediction. With the exception of one outlier, all the data fall within the prediction bounds of a horizontal line. To test if a linear regression was appropriate to summarize these data we also fit exponential and quadratic functions. Application of Akaike’s information criteria for model selection revealed that these data are best represented with a horizontal line [17] (the AIC scores for the linear, quadratic and exponential fits were 3.5, 5.3 and 5.2, respectively). This demonstrates that shape polarity has no detectable effect on measures of amplification. The implication is that the underlying biochemical network acts as a linear amplifier over the range of inputs considered in the micropipette assay. We note that this does not prove that the biochemical network is linear across all possible input values. Just as all electrical linear amplifiers have

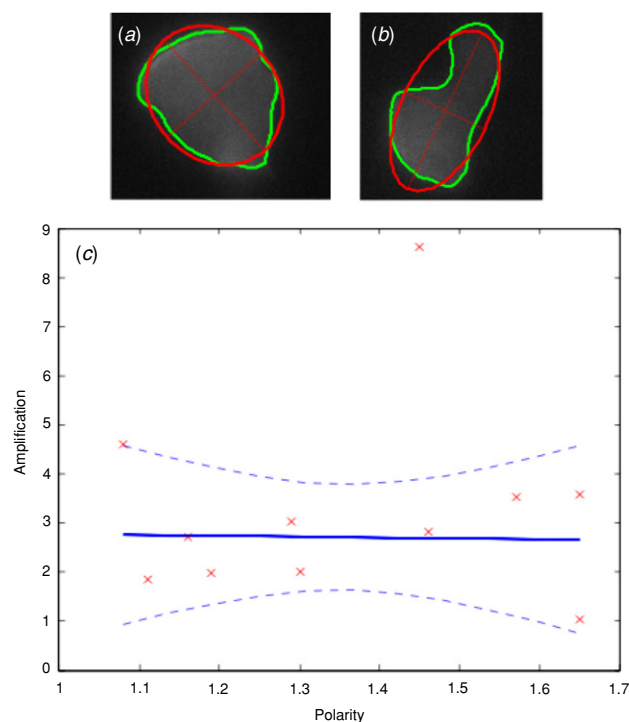


Figure 5. Amplification is not correlated with shape polarity. Polarity is calculated by first fitting an ellipse to the shape data, and then taking the ratio of the major and minor axes. (a) An example of cell with polarity of 1.18. (b) An example of cell with polarity of 1.9. (c) Amplification does not depend on shape polarity.

regions of nonlinearity (e.g., saturation), there are likely inputs that cause nonlinear or polarity-dependent amplification in HL60s. However, we did not see these nonlinear effects in the micropipette assay, which is a common assay measuring PIP3 amplification. Here the input was controlled by the cell polarity, which varied by $\pm 21\%$ about the mean.

Conclusion and outlook

In this study we have measured amplification in the HL60 chemotaxis network and demonstrated the role of morphology in PIP3 localization. We confirmed that there is indeed more membrane at the front of chemotaxing HL60s and that this asymmetric distribution of membrane contributes to the PIP3 amplification. If the distribution of membrane is ignored, then there will be a significant overestimation of the biochemical amplification. Our value of the true amplification of the network is 3.25 ± 2.0 which is in close agreement with the value 3.1 ± 0.9 reported by [2] for latrunculin-treated *D. discoideum*. The value of amplification reported for latrunculin-treated HL60s [12], which is approximately 1.3, also falls within our range for the membrane-normalized amplification. However, as we noted above, the authors of [12] used a different method of data extraction than that we used, which will cause some discrepancy in comparing our amplification values. When we ignored the membrane distribution the value of amplification was 5.34 ± 2.5 , which

gives an approximately 50% difference between this value and the true biochemical amplification.

These results suggest that the previously reported differences in amplification between polarized and latrunculin-treated cells [2, 12] are due, in part, to a difference in membrane distribution. There are at least three possible ways through which the actin cytoskeleton causes an asymmetric membrane distribution. First is the membrane ruffling at the leading edge caused by actin filament reorganization [18]. Second, the actin cytoskeleton is necessary for vesicular trafficking, which affects membrane redistribution [19]. And third, our data show that a chemotaxing cell is taller at the front than at the back; the cell shown in figure 4(c) is at least 47% taller at its leading edge than at its trailing edge (it may be taller, but the five images on the top of the Z-stacks were discarded because they could not be reliably segmented). This difference in cell height places more membrane at the leading edge. When a cell is treated with latrunculin these processes are inhibited and therefore the cell will have a more uniform membrane distribution. Our results demonstrate that much of the difference in amplification between polarized and unpolarized cells can be explained by difference in membrane localization. We attempted to repeat our experiments in the presence of latrunculin but our cells did not localize PIP3 to the membrane. We suspect that the combination of our transfected chimera proteins and latrunculin treatment inhibited the PIP3 signaling pathway.

As a final result, we found that there is no association between shape polarity and amplification. Based on our theoretical results we conclude that the biochemical network behaves as a linear amplifier over the range of inputs we considered.

Together, these results demonstrate that morphology is an important engineering parameter for this amplification and cellular guidance system. The effect is large enough to reduce the need to invoke a biochemical feedback from the actin polymerization system to the signaling system to explain the difference in amplification in untreated and latrunculin-treated cells. Furthermore, an asymmetric distribution of membrane is also likely to increase the persistence of a chemotaxing cell by making the established front more sensitive than the back and sides of the cell. Finally, the discovery that the underlying biochemical network likely functions as a linear amplifier puts constraints on the structure and parameters of the underlying signaling network.

Acknowledgments

We thank Christopher Rao for insightful discussions of the paper, in particular for giving the conditions under which shape polarity will affect amplification, and Alexandra Van Keymeulen for teaching MDO the micropipette assay. We also thank Shilpa Shroff and Keith Erickson for their feedback. MDO and APA would like to thank the Howard Hughes Medical Institute and the NIH for funding and the Alliance for Cellular Signaling for providing constructs and advice during the course of this research. KW was a postdoctoral fellow of the American Heart Association.

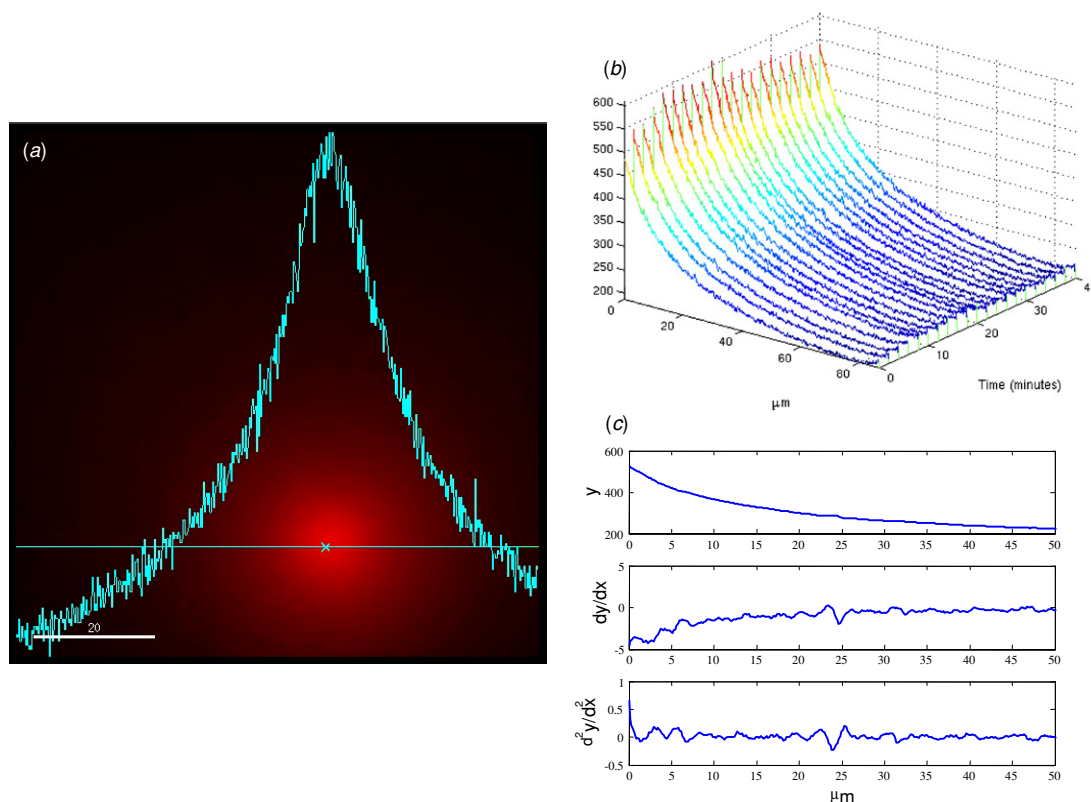


Figure A.1. Characterization of the micropipette gradient. (a) An image of Texas red diffusing from a micropipette. The horizontal intensity profile is shown in cyan. (b) The radial intensity profiles obtained from a 60 min experiment with images taken every minute. The concentration profile remained stable for 45 min. The first 15 min were spent adjusting the back pressure on the micropipette (see the inset for all data). (c) Analysis of chemical field. (Top) The radial intensity of Texas Red diffusing from the micropipette versus distance (μm) from tip. (Middle) First derivative of the data from the top plot. (Bottom) Second derivative of the data from the top plot.

Appendix A

Effect of cell shape on amplification

Here we analyze how cell shape affects amplification in general vector-sum directional sensing models [24]. Consider a cell of arbitrary shape immersed in a chemoattractant field, $l(x, y)$. At each point on the cell's boundary the chemoattractant concentration is transduced into an internal signal. We represent this transduction by the scalar function $\phi(\cdot)$. The vector integral of $\phi(l(x, y))$ over the cell's surface area gives the direction and magnitude of the internal 'compass' \vec{s} , which is analogous to PIP3. This general vector sum can be represented by the following equation:

$$\vec{s} = \int_A \phi[l(x, y)] \vec{n}(x, y) dA, \quad (\text{A.1})$$

where $\vec{n}(x, y)$ is the normal vector at point (x, y) . Application of the fundamental theorem of calculus ($f(x) = \frac{d}{dx} \int_a^x f(t) dt$) along each dimension of \vec{n} and mean value theorem leads to

$$\vec{s} = V \langle \nabla \phi[l(x, y)] \rangle. \quad (\text{A.2})$$

Equation (A.2) states that the output of our general directional sensing model, \vec{s} , is equal to the volume of the cell times the mean value of the gradient of the internal signal, $\phi[l(x, y)]$.

This form of the equation gives insight into when cell morphology will affect cell signaling. For example, when the function $\phi[l(x, y)]$ is linear then \vec{s} becomes independent of the spatial coordinates. For example when the cell is in a linear gradient ($l(x, y) = mx + my$) and $\phi(\cdot)$ is constant ($\phi = k$). Equation (A.2) reduces to

$$\vec{s} = kmV(\vec{i} + \vec{j}) \quad (\text{A.3})$$

(where \vec{i} and \vec{j} are unit coordinate vectors). While the magnitude of \vec{s} does depend on the volume V , there is no evidence that the cell significantly changes its volume during chemotaxis⁶ [25]; therefore, we conclude that in this situation signaling does not depend on cell shape. In fact, anytime that $\phi[l(x, y)]$ is linear, \vec{s} will not depend on cell shape; so the question becomes when is it linear? In the next section we show that the concentration field produced by a micropipette is approximately linear across the length of the cell when cell is not next to the micropipette. Therefore $\phi[l(x, y)]$ is nonlinear only if $\phi(\cdot)$ is a nonlinear function. This implies that shape polarity will lead to amplification only if $\phi(\cdot)$ is nonlinear.

⁶ It was shown in [2] that when a leukocyte is brought from resting to a turgid state, the volume of the cell can increase by as much as 60%. However, turgid conditions are not physiologically relevant for chemotaxis.

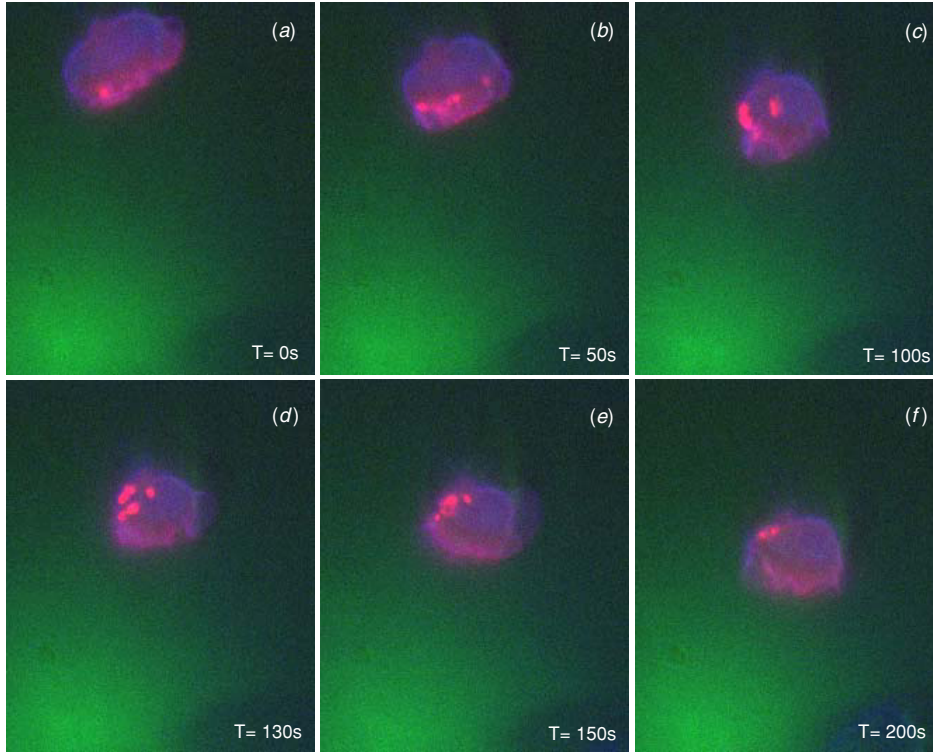


Figure B.1. Bright, PH-Akt-YFP-rich macropinosomes are found in 5 of 16 chemotaxis experiments. (a)–(f) A time course of HL60 crawling up fMLP gradient (green). CFP-CAAX (blue) and PH-Akt-YFP (red) were used to label the plasma membrane and PIP3, respectively. The bright dots start at the leading edge ((a) and (b)) and then move along the periphery toward the back of the cell ((c)–(f)) where they remain while the cell moves.

The gradient produced by a micropipette appears linear to a cell when the cell is not near the micropipette tip

We model the diffusion of chemoattractant from a micropipette as diffusion from a point source [26]. The steady-state concentration as a function of distance is given by

$$l(r) = \frac{q}{4\pi Dr}, \quad (\text{A.4})$$

where l is the concentration (mol cm^{-3}), q is the rate of release of the peptide, D is the diffusion coefficient and r is the distance (cm) from the point source. The concentration gradient is given by

$$\nabla l(r) = \frac{c_r}{r^2}, \quad (\text{A.5})$$

where we lumped all the parameters into the constant c_r . Consider the change in the gradient at r due to a perturbation ε :

$$\nabla l(r - \varepsilon) - \nabla l(r) = \frac{c_r}{(r - \varepsilon)^2} - \frac{c_r}{r^2}. \quad (\text{A.6})$$

Expanding the right-hand side of equation (A.3) we get the following equation for the change in gradient about ε :

$$\frac{2c_r\varepsilon}{r^3} + O[\varepsilon/r]^2. \quad (\text{A.7})$$

For $\varepsilon \ll r$, equation (A.4) will be approximately zero; thus the gradient will be approximately constant (linear chemical field). However, as r approaches zero (when the cell is near

the micropipette), then $\varepsilon \sim O[r]$ and the chemical field will be nonlinear. Let ε be the diameter of the cell. This analysis implies that the chemical field will appear approximately linear except when the cell is close to the micropipette.

Figure A.1 shows the chemical field produced by a micropipette. In this case, a mixture of Texas Red and fMLP are diffusing out of the tip. Figure A.1(a) shows the fluorescent distribution in red and how this intensity changed along a horizontal line through the micropipette tip in cyan (length scale is shown at the bottom left corner in microns). Figure A.1(b) shows how this radial intensity varied with time in a 45 min experiment, where an image was taken every minute. We see that the chemoattractant gradient remained relatively stable for 45 min.

We now check whether the chemical distribution appears linear across the length of the cell. For a worst case analysis, we take the steepest profile from figure A.1(b) and numerically compute its derivative. This is shown in figure A.1(c). We next evaluate where the difference in the gradient across the length of the cell (approximately $10 \mu\text{m}$) is greater than zero. We see that this occurs only when the cell is within $10 \mu\text{m}$ of the micropipette tip. Therefore we conclude that the chemical field will appear linear to the cell except when it is within $10 \mu\text{m}$ of the micropipette tip. We can also check this by looking at the second derivative. We see in the bottom subplot of figure A.1(c) that the second derivative is essentially zero, except right next to the micropipette.

Appendix B

Existence of macropinosomes

In 5 of our 16 micropipette experiments we found that the cells exhibited high levels of macropinocytosis [27]. Since macropinosomes are known to be dense with PIP3 they are also dense with PH-Akt-YFP. Figure B.1 shows one such experiment, where the fMLP gradient is shown in green, the receptor distribution in blue and the PH-Akt in red. Figure B.1(a) shows the formation of a pinosome near the leading edge and figures B.1(b)–(f) show how this macropinosome and others were sorted at the back of the cell. Since these bright macropinosomes stayed near the cell boundary, they obscured our measurements of amplification. Therefore, we did not include these cells in the analysis presented in this paper.

Glossary

Amplification. A measure of the increase in signal strength of an amplifier circuit (electronic or biochemical). Here, amplification is the per cent change in a biochemical circuit's output divided by the per cent change in its input.

Chemotaxis. The characteristic movement of an organism or cell along a chemical concentration gradient toward the chemical stimulus.

Morphology. The form and structure of an organism. Here, we are concerned with the geometric shape of the cell and its distribution of plasma membrane.

Phosphatidylinositol (3,4,5)-trisphosphate (abbreviated PIP3). PIP3 is the product of the class I phosphoinositide 3-kinases (PI 3-kinases) activity on Phosphatidylinositol (4,5)-bisphosphate. PIP3 is an important signaling lipid involved in chemotaxis and cell growth.

formyl-Met-Leu-Phe (abbreviated fMLP). fMLP is a synthetic peptide that mimics the activity of bacterially-derived peptides with formylated N-terminal methionine groups. These peptides are attractants for leukocytes.

References

- [1] Devreotes P N and Zigmond S H 1988 Chemotaxis in eukaryotic cells: a focus on leukocytes and Dictyostelium *Annu. Rev. Cell Biol.* **4** 649–86
- [2] Janetopoulos C *et al* 2004 Chemoattractant-induced phosphatidylinositol 3,4,5-trisphosphate accumulation is spatially amplified and adapts, independent of the actin cytoskeleton *Proc. Natl Acad. Sci. USA* **101** 8951–6
- [3] Servant G *et al* 1999 Dynamics of a chemoattractant receptor in living neutrophils during chemotaxis *Mol. Biol. Cell* **10** 1163–78
- [4] Srinivasan S *et al* 2003 Rac and Cdc42 play distinct roles in regulating PI(3,4,5)P3 and polarity during neutrophil chemotaxis *J. Cell Biol.* **160** 375–85
- [5] Funamoto S *et al* 2002 Spatial and temporal regulation of 3-phosphoinositides by PI 3-kinase and PTEN mediates chemotaxis *Cell* **109** 611–23
- [6] Iijima M and Devreotes P 2002 Tumor suppressor PTEN mediates sensing of chemoattractant gradients *Cell* **109** 599–610
- [7] Koshland D E Jr, Goldbeter A and Stock J B 1982 Amplification and adaptation in regulatory and sensory systems *Science* **217** 220–5
- [8] Ma L *et al* 2004 Two complementary, local excitation, global inhibition mechanisms acting in parallel can explain the chemoattractant-induced regulation of PI(3,4,5)P3 response in dictyostelium cells *Biophys. J.* **87** 3764–74
- [9] Weiner O D 2002 Regulation of cell polarity during eukaryotic chemotaxis: the chemotactic compass *Curr. Opin. Cell Biol.* **14** 196–202
- [10] Devreotes P and Janetopoulos C 2003 Eukaryotic chemotaxis: distinctions between directional sensing and polarization *J. Biol. Chem.* **278** 20445–8
- [11] Levchenko A and Iglesias P A 2002 Models of eukaryotic gradient sensing: application to chemotaxis of amoebae and neutrophils *Biophys. J.* **82** 50–63
- [12] Wang F *et al* 2002 Lipid products of PI(3)Ks maintain persistent cell polarity and directed motility in neutrophils *Nat. Cell Biol.* **4** 513–8
- [13] Servant G *et al* 2000 Polarization of chemoattractant receptor signaling during neutrophil chemotaxis *Science* **287** 1037–40
- [14] Farrell B E, Daniele R P and Lauffenburger D A 1990 Quantitative relationships between single-cell and cell-population model parameters for chemosensory migration responses of alveolar macrophages to C5a *Cell Motil. Cytoskeleton* **16** 279–93
- [15] Haribabu B *et al* 2000 Function and regulation of chemoattractant receptors *Immunol. Res.* **22** 271–9
- [16] Holland P W and Welsch R E 1977 Robust regression using iteratively reweighted least-squares *Commun. Stat.—Theory Methods A* **6** 813–27
- [17] Burnham K P and Anderson D R 2002 *Model Selection and Multimodel Inference* 2nd edn (Berlin: Springer)
- [18] Borm B *et al* 2005 Membrane ruffles in cell migration: indicators of inefficient lamellipodia adhesion and compartments of actin filament reorganization *Exp. Cell Res.* **302** 83–95
- [19] Alberts B *et al* 2002 *Molecular Biology of the Cell* 4th edn (New York: Garland Science)
- [20] Servant G *et al* 2000 Polarization of chemoattractant receptor signaling during neutrophil chemotaxis *Science* **287** 1037–40
- [21] Srinivasan S *et al* 2003 Rac and Cdc42 play distinct roles in regulating PI(3,4,5)P3 and polarity during neutrophil chemotaxis *J. Cell Biol.* **375**–85
- [22] Servant G *et al* 1999 Dynamics of a chemoattractant receptor in living neutrophils during chemotaxis *Mol. Biol. Cell* **10** 1163–78
- [23] Kass M, Witkin A and Terzopoulos D 1987 Snakes: active contour models *Int. J. Comput. Vis.* **1** 321–31
- [24] Foxman E F, Kunkel E J and Butcher E C 1999 Integrating conflicting chemotactic signals: the role of memory in leukocyte navigation *J. Cell Biol.* **147** 577–88
- [25] Schmid-Schonbein G W, Shih Y Y and Chien S 1980 Morphometry of human leukocytes *Blood* **56** 866–75
- [26] Crank J 1975 *The Mathematics of Diffusion* (Oxford: Clarendon)
- [27] Amyere M *et al* 2002 Origin, originality, functions, subversions and molecular signalling of macropinocytosis *Int. J. Med. Microbiol.* **291** 487–94